International Journal of Solids and Structures 48 (2011) 2565–2575

Contents lists available at ScienceDirect

International Journal of Solids and Structures

journal homepage: www.elsevier.com/locate/ijsolstr

Mechanics of non-slipping adhesive contact on a power-law graded elastic half-space

Xu Guo [a,*], Fan Jin [a], Huajian Gao [b,*]

[a] State Key Laboratory of Structural Analysis for Industrial Equipment, Department of Engineering Mechanics, Dalian University of Technology, Dalian 116023, PR China
[b] Division of Engineering, Brown University, Providence, RI 02912, USA

ARTICLE INFO

Article history:
Received 22 January 2011
Received in revised form 3 April 2011
Available online 18 May 2011

Keywords:
Contact mechanics
Normal/tangential coupling
Elastic power-law graded material
Negative Poisson's ratio
Mode mixity

ABSTRACT

In previous work about axisymmetric adhesive contact on power-law graded elastic materials, the contact interface was often assumed to be frictionless, which is, however, not always the case in practical applications. In order to elucidate the effect of friction and the coupling between normal and tangential deformations, in the present paper, the problem of a rigid punch with a parabolic shape in non-slipping adhesive contact with a power-law graded half-space is studied analytically via singular integral equation method. A series of closed-form analytical solutions, which include the frictionless and homogeneous solutions as special cases, are obtained. Our results show that, compared with the frictionless case, the interfacial friction tends to reduce the contact area and the indentation depth during adhesion. The magnitude of the coupling effect depends on both the Poisson ratio and the gradient exponent of the half-space. This effect vanishes for homogeneous incompressible as well as for linearly graded materials but becomes significant for auxetic materials with negative Poisson's ratio. Furthermore, influence of mode mixity on the adhesive behavior of power-law graded materials, which was seldom touched in literature, is discussed in details.

1. Introduction

Mechanics of functionally graded materials (FGMs) with spatially varying elastic moduli is of significance to many applications in tribology (Enomoto and Yamamoto, 1998; Donnet and Erdemi, 2004), adhesion (Giannakopoulos and Pallot, 2000; Chen et al., 2009b), geology (Holl, 1940; Booker et al., 1985a,b), biomechanics (Pompe et al., 2003; Hedia and Nemat-Alla, 2004), fracture mechanics (Suresh, 2001), thermo-mechanical systems (Pindera et al., 1998; Nemat-Alla, 2003), energy storage/conversion systems (Kambe and Shikata, 2003; Kato et al., 2006) and nanotechnology (Li et al., 2009; Sioh, 2010). In particular, the contact mechanics of FGMs has received considerable attention in the past (Giannakopoulos and Pallot, 2000). Early studies on the contact mechanics of FGMs focused on the settlement of foundations on soils with elastic moduli varying linearly with depth (Holl, 1940; Lekhnitskii, 1962; Gibson, 1967; Gibson and Sills, 1975; Calladine and Greenwood, 1978; Booker et al., 1985a,b). More recent studies have demonstrated that FGMs can be designed to have substantially improved resistance to contact damage compared to their homogeneous counterpart (Suresh and Mortensen, 1998; Suresh, 2001). Suresh and coworkers made systematic investigations on the mechanics of indentation on graded elastic solids (Giannakopoulos and Suresh, 1997a,b; Giannakopoulos and Pallot, 2000; Choi et al., 2008; Prasad et al., 2009), and proposed a theoretical framework for frictionless contact of graded materials under concentrated point loads and axisymmetric indenters (Giannakopoulos and Suresh, 1997a,b). The plane strain problem of a rigid cylinder in contact with a power-law graded half-space was also examined by Giannakopoulos and Pallot (2000).

With the rapid development of nanotechnology, micro- and nano-indentation has become a powerful tool to characterize mechanical properties of a variety of biological/soft materials with sizes approaching molecular or atomic dimension. For such application, the adhesion forces between contact surfaces induced by capillary, electrostatic and van der Waals interactions will come into play and may affect the contact behavior significantly. Recent years have witnessed a continuously growing interest in adhesive contact between soft materials from different branches of engineering and applied sciences. Compared with studies on adhesive contact mechanics of homogeneous materials (Johnson et al., 1971; Derjaguin et al., 1975; Barquins, 1988; Maugis, 1992; Chaudhury et al., 1996; Baney and Hui, 1997; Greenwood, 1997; Barthel, 1998; Hui et al., 2001; Chen and Gao, 2006a,b, 2007a,b), there is so far only limited work (Giannakopoulos and Pallot, 2000; Chen et al., 2009b; Jin and Guo, 2010) on adhesive

* Corresponding authors.
E-mail addresses: guoxu@dlut.edu.cn (X. Guo), Huajian_Gao@brown.edu (H. Gao).

0020-7683/$ - see front matter © 2011 Elsevier Ltd. All rights reserved.
doi:10.1016/j.ijsolstr.2011.05.008

contact of graded materials in spite of their growing importance for biological and soft material systems. Giannakopoulos and Pallot (2000) proposed an energy-based approach to two-dimensional adhesive contact on power-law graded materials. Recently, Chen et al. (2009b) studied frictionless adhesive contact between a rigid sphere and a power-law graded elastic half-space and, rather amazingly, obtained a number of simple closed-form analytical solutions to a seemingly very complex problem. A problem of the solutions presented in Chen et al. (2009b) is that the coupling between normal and tangential deformations within the contact region are ignored, which might seriously limit their applications to many practical cases in which friction forces may play an important role.

The present paper is aimed to develop a series of closed-form analytical solutions for non-slipping adhesive contact between a rigid punch and a power-law graded elastic half-space. Our work makes two critical contributions to adhesive contact mechanics. First, we develop fundamental analytical solutions to non-slipping adhesive contact on power-law graded materials which can capture the contact behaviors of a broad range of soft materials in biology and engineering. Second, as shown by Waters and Guduru (2010), the effect of mode mixity is a critical factor for the analysis of adhesive contact between soft materials, which obviously cannot be addressed in a theoretically consistent way if the coupling between normal and tangential deformations within the contact region is ignored, as in Chen et al. (2009a,b).

The rest of the paper is organized as follows. In Section 2, the non-slipping adhesive contact problem is formulated as a set of coupled Abel-type singular integral equations and the corresponding solution procedure is presented. In Section 3, we show that the solutions are available in closed form by the Jacobi polynomial method. As an important degenerate case, a generalized non-slipping JKR model for homogeneous half-space is examined and compared with the classical JKR model in Section 4. The model of an adhesion mediated deformation sensor proposed in Chen and Gao (2006b) is extended to power-law graded materials in Section 5. In Section 6, the influence of mode mixity on adhesive contact of graded materials is discussed in the plane strain case. Definitions of the corresponding stress intensity factor and energy release rate, which generalize the classical results for homogeneous materials, are also presented in this section. Some concluding remarks are given in Section 7.

2. Problem statement and the solution approach

Consider a rigid punch in *non-slipping* adhesive contact with an isotropic, power-law graded elastic half-space (Fig. 1). The profile of the rigid punch is assumed to have the following form

$$f(r)=\sum_{n_1=0}^{N_1}\frac{\alpha_{n_1}r^{2n_1}}{R^{2n_1-1}}\quad (N_1=0,1,2,\ldots), \tag{1}$$

where $a_{n_1}\geqslant 0$ is a dimensionless parameter and R is a characteristic length. The case $N_1=1$ and $\alpha_0=0$, $\alpha_1=1/2$ corresponds to the parabolic shape used in most of the classical contact models to approximate a sphere of radius R when the contact radius is small (Johnson, 1985). It is assumed that the Poisson ratio of the half-space has a constant value v in the interval $[-1,0.5]$, while its Young's modulus varies in the power-law form

$$E=E_0(z/c_0)^k,\quad 0<k<1, \tag{2}$$

where $E_0>0$ is a reference modulus, $c_0>0$ is a characteristic depth and k is the gradient exponent. The system is subjected to a normal contact force P (negative when tensile) applied on the rigid sphere and a mismatch strain distribution $\varepsilon(r)$ between the contact surfaces in the following form

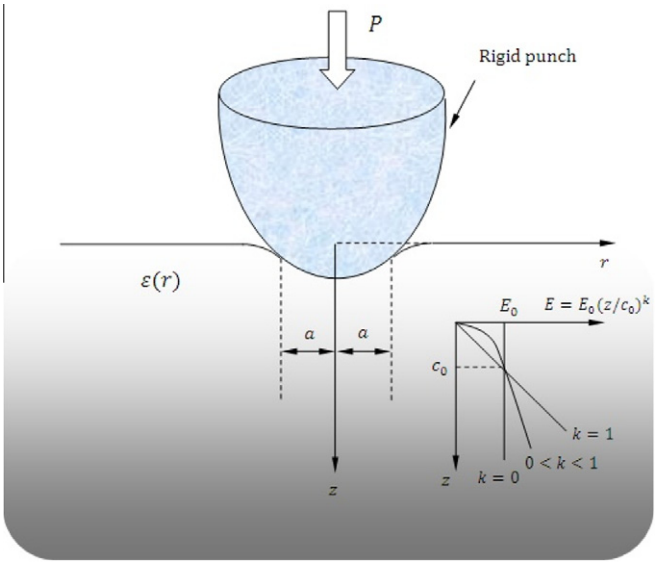

Fig. 1. Schematic illustration of a rigid punch in non-slipping contact with a power-law graded elastic half-space under a normal force P and a mismatch strain $\varepsilon(r)$.

$$\varepsilon(r)=-\sum_{n_2=0}^{N_2}(n_2+1)\varepsilon_{n_2}\left(\frac{r}{R}\right)^{n_2}\quad (N_2=0,1,2,\ldots), \tag{3}$$

where ε_{n_2} is a dimensionless parameter. This type of mismatch strain distribution could be induced by a non-uniform temperature change in the radial direction (Chen and Gao, 2006b). The case $N_2=0$ corresponds to a constant mismatch strain. Due to the non-slipping condition, both normal and tangential interfacial tractions will be induced by the adhesion between the two objects. The radius of the contact region is denoted by a.

Using the surface elastic Green's function, the relation between the surface displacements of the half-space ($\bar{u}_r(r)=-\int_0^r\varepsilon(s)\mathrm{d}s$ and $\bar{u}_z(r)$) and the corresponding interfacial tractions within the contact region ($p(r)=\sigma_{zz}(r)$ and $q(r)=\tau_{rz}(r)$) can be established as follows (Popov, 1973):

$$\int_{-a}^{a}[K_k(x-s)-K_k(-s)]\chi(s)\mathrm{d}s=H(x), \tag{4}$$

where

$$K_k(s)=|s|^{-k}\left[\mathrm{sign}(s)+\mathrm{i}\tan\frac{\lambda\pi}{2}\left(\cot\frac{k\pi}{2}\right)^2\right],\ \chi(s)=\kappa^{\frac{1}{2}}p^*(s)+\mathrm{i}\kappa^{-\frac{1}{2}}q^*(s),$$
$$H(x)=\frac{2x\tan(\lambda\pi/2)}{\pi\theta_1\sqrt{\kappa}\tan(k\pi/2)}\int_0^1\frac{[\bar{u}_z(xt)t+\mathrm{i}\kappa\bar{u}_r(xt)]}{\sqrt{1-t^2}}\mathrm{d}t \tag{5}$$

with $\mathrm{i}=\sqrt{-1}$ and

$$\lambda=\beta-1,\quad \kappa=\frac{\beta}{1+k},\quad \beta=\sqrt{(1+k)\left(1-\frac{kv}{1-v}\right)},$$
$$\theta_1=-\frac{c_0^kC_k\cos\frac{\beta\pi}{2}}{kE^*},\quad E^*=\frac{E_0}{1-v^2},\quad C_k=\frac{2^{1+k}\Gamma\left(\frac{3+k+\beta}{2}\right)\Gamma\left(\frac{3+k-\beta}{2}\right)}{\pi\Gamma(2+k)},$$
$$p^*(s)=\frac{2}{\pi}\int_s^a\frac{tp(t)\mathrm{d}t}{\sqrt{t^2-s^2}},\quad q^*(s)=\frac{2s}{\pi}\int_s^a\frac{q(t)\mathrm{d}t}{\sqrt{t^2-s^2}}, \tag{6}$$

where $\Gamma(\cdot)$ denotes the Gamma function.

Under the prescribed interfacial displacements $\bar{u}_r(r)$ and $\bar{u}_z(r)$, Eq. (4) is a set of coupled Abel type singular integral equations for unknown interfacial tractions, $p(r)$ and $q(r)$. Note that the

normal and tangential deformations are fully coupled in the above formulation.

According to Popov (1973), the exact solution of the integral equation in Eq. (4) can be expressed as a series of Jacobi polynomials, that is

$$\chi(x)=\sum_{m=0}^{\infty}\frac{\chi_m P_m^{\rho}(x)}{\psi_{\rho}(x)}, \tag{7}$$

where $P_m^{\rho}(x)=P_m^{k/2-i\rho,k/2+i\rho}(x/a)$ is the Jacobi polynomial of order m with index $(k/2-i\rho,k/2+i\rho)$ and

$$\begin{aligned}\chi_m&=\frac{(m!)^2(1+k+2m)\Gamma(k)\sin(k\pi/2)\cosh(\pi\rho)}{\pi(2a)^{1+k}|\Gamma(1+m+k/2+i\rho)|^2}H_m,\\ H_m&=\int_{-a}^{a}\frac{H'(x)P_m^{-\rho}(x)}{\psi_{-\rho}(x)}\mathrm{d}x,\quad m=0,1,2,\ldots,\\ \psi_{\rho}(x)&=(a-x)^{-\frac{k}{2}+i\rho}(a+x)^{-\frac{k}{2}-i\rho},\quad \rho=\frac{1}{2\pi}\ln\frac{\sin[(k+\lambda)\pi/2]}{\sin[(k-\lambda)\pi/2]},\end{aligned} \tag{8}$$

where $H'(x)=\mathrm{d}H/\mathrm{d}x$. Once $\chi(x)$ is determined, the interfacial tractions $p(r)$ and $q(r)$ can be obtained from its real and imaginary parts through

$$\begin{aligned}rp(r)&=-\kappa^{-\frac{1}{2}}\frac{\mathrm{d}}{\mathrm{d}r}\int_r^a\frac{s\mathrm{Re}[\chi(s)]}{\sqrt{s^2-r^2}}\mathrm{d}s,\\ q(r)&=-\kappa^{\frac{1}{2}}\frac{\mathrm{d}}{\mathrm{d}r}\int_r^a\frac{\mathrm{Im}[\chi(s)]}{\sqrt{s^2-r^2}}\mathrm{d}s,\end{aligned} \tag{9}$$

respectively.

Accordingly, the force applied on the punch can be expressed as

$$P=\frac{\sin(k\pi/2)\cosh(\pi\rho)}{k\sqrt{\kappa}}\mathrm{Re}[H_0]. \tag{10}$$

The surface energy associated with the contact region can be expressed as

$$U_s=-\pi a^2\Delta\gamma, \tag{11}$$

where $\Delta\gamma$ is the work of adhesion that could include possible energy dissipation during the adhesion process.

The total free energy of the system is taken to be

$$U_T=U_E+U_s, \tag{12}$$

where U_E denotes the elastic strain energy stored in the graded half-space. The contact radius a is then determined from (Giannakopoulos and Pallot, 2000; Chen et al., 2009b)

$$\left.\frac{\partial U_T}{\partial a}\right|_{\delta,\varepsilon}=0 \tag{13}$$

for fixed values of δ and ε.

In the following sections, the above solution procedure will be employed to investigate a rigid punch in non-slipping adhesive contact with a power-law graded elastic half-space, taking into account the full coupling between normal and tangential deformations.

3. Explicit solutions

From Eqs. (1) and (3), the axisymmetric surface displacements of the half-space under the indentation of a rigid punch and the distributed mismatch strain can be written as

$$\bar{u}_z(r)=\delta-\sum_{n_1=0}^{N_1}\frac{\alpha_{n_1}r^{2n_1}}{R^{2n_1-1}},\quad \bar{u}_r(r)=\sum_{n_2=0}^{N_2}\frac{\varepsilon_{n_2}r^{n_2+1}}{R^{n_2}},\quad |r|<a, \tag{14}$$

where δ is the depth of indentation.

Inserting Eq. (14) into Eq. $(5)_3$, and then into Eq. $(8)_2$ yields

$$\begin{aligned}H_m=\frac{2\tan(\lambda\pi/2)}{\pi\theta_1\sqrt{\kappa}\tan(k\pi/2)}\Bigg[&\delta\Theta(0,m)\\ &-\sum_{n_1=0}^{N_1}\alpha_{n_1}\frac{\sqrt{\pi}(1+2n_1)}{2R^{2n_1-1}}\frac{\Gamma(1+n_1)}{\Gamma(3/2+n_1)}\Theta(2n_1,m)\\ &+\frac{i\kappa\sqrt{\pi}}{2}\sum_{n_2=0}^{N_2}\frac{(2+n_2)\Gamma(1+n_2/2)\varepsilon_{n_2}}{\Gamma(3/2+n_2/2)R^{n_2}}\Theta(1+n_2,m)\Bigg],\end{aligned} \tag{15}$$

where

$$\Theta(n,m)=\int_{-a}^{a}\frac{x^nP_m^{-\rho}(x)}{\psi_{-\rho}(x)}\mathrm{d}x\quad(m,n=0,1,2,\ldots). \tag{16}$$

Since

$$\Theta(n,m)=\begin{cases}\sum_{j=m}^{n}(-1)^{j+m}\Delta_n^j\Delta_j^m\frac{2^{1+j+k}\Gamma\left(1+j+\frac{k}{2}+i\rho\right)\Gamma\left(1+m+\frac{k}{2}-i\rho\right)}{\Gamma(j+k+m+2)}a^{n+1+k}, & 0\leqslant m\leqslant n,\\ 0, & m\geqslant n+1,\end{cases} \tag{17}$$

where $\Delta_n^j=n!/[j!(n-j)!]$, it can be seen from Eqs. (15) and (17) that for any prescribed $N_1\geqslant 0$ and $N_2\geqslant 0$, there will be only finite non-zero terms of χ_m in Eq. (7). This means that closed-form analytical solutions for the considered problem are available as long as the shape $f(r)$ of the axisymmetric punch and the mismatch strain distribution $\varepsilon(r)$ can be described in the form of Eqs. (1) and (3), respectively. However, the solution procedure can be quite lengthy when N_1 and N_2 are large. For the sake of simplicity, we will only focus on the case of parabolic shape punch ($\alpha_2=1/2$ and all other $\alpha_{n_1}=0$) and constant mismatch strain $N_2=0$ in the following text.

3.1. Stress fields within the contact zone

For a rigid punch with a parabolic shape $f(r)=r^2/2R$ and a constant mismatch strain, combining Eqs. (7), $(8)_1$, (9), (15) and (17) leads to the following explicit expressions for $p(r)$ and $q(r)$

$$\begin{aligned}rp(r)&=-d_1\Phi_1'(r)+\frac{d_3}{\kappa}\Phi_3'(r)+\frac{d_2d_3}{\kappa}\Psi_2'(r),\\ q(r)&=-\kappa d_1\Psi_0'(r)+d_3\Psi_2'(r)-d_2d_3\Phi_1'(r),\end{aligned} \tag{18}$$

where

$$\begin{aligned}d_1&=\frac{P\Gamma(2+k)}{\pi(2a)^{1+k}R_t}+\frac{d_3}{\kappa}\left(\frac{1+4\rho^2}{3+k}a^2+2\kappa\rho Ra\varepsilon\right),\\ d_2&=2\rho a+(2+k)\kappa R\varepsilon,\\ d_3&=\frac{4E^*\cos(k\pi/2)\cosh(\pi\rho)}{(1+k)(2+k)\pi^2c_0^kRC_k\sin(\beta\pi/2)},\quad R_t=\left|\Gamma\left(1+\frac{k}{2}+i\rho\right)\right|^2\end{aligned} \tag{19}$$

with

$$\begin{aligned}\Phi_n'(r)&=\frac{\mathrm{d}}{\mathrm{d}r}\int_r^a\frac{s^n(a^2-s^2)^{\frac{k}{2}}}{\sqrt{s^2-r^2}}\cos\left(\rho\ln\frac{a+s}{a-s}\right)\mathrm{d}s,\\ \Psi_n'(r)&=\frac{\mathrm{d}}{\mathrm{d}r}\int_r^a\frac{s^n(a^2-s^2)^{\frac{k}{2}}}{\sqrt{s^2-r^2}}\sin\left(\rho\ln\frac{a+s}{a-s}\right)\mathrm{d}s,\quad n=0,1,2,3.\end{aligned} \tag{20}$$

It can be verified that the interfacial tractions $p(r)$ and $q(r)$ obtained above satisfy the boundary conditions:

$$\begin{aligned}&P=2\pi\int_0^a rp(r)\mathrm{d}r,\quad \int_0^{2\pi}\int_0^a rq(r)\cos\theta\,\mathrm{d}r\,\mathrm{d}\theta=0,\\ &\int_0^{2\pi}\int_0^a rq(r)\sin\theta\,\mathrm{d}r\,\mathrm{d}\theta=0.\end{aligned} \tag{21}$$

It can be seen from the above results that, in contrast to the frictionless contact solution (Giannakopoulos and Suresh, 1997b; Chen et al., 2009b), the singular stress field in Eq. (18) oscillates

with increasing frequency near the contact edge. This character is due to the coupling between normal and tangential deformations induced by the non-slipping condition in the contact region. The above analysis also reveals that the magnitude of this coupling effect is controlled by the parameter defined in Eq. $(8)_4$, which is a generalized version of the oscillation index (Williams, 1959) for power-law graded materials. The larger the value of ρ, the stronger the coupling effect. The oscillatory stress field is analogous to that near the tip of an interfacial crack in dissimilar media (Rice, 1988; Hutchinson and Suo, 1992). As also pointed out by Johnson (1985), this anomalous behavior is mainly due to the fact that linear elasticity theory is not adequate to handle the high strain gradients near the contact edge. On the other hand, the oscillatory stress field is expected to hold away from a small singular zone around the contact edge.

Fig. 2 depicts the variation of the coupling coefficient ρ with respect to the gradient exponent k for a set of Poisson's ratio v. It shows that for homogeneous incompressible material ($k = 0$ and $v = 0.5$) and linearly graded material ($k = 1$), the coupling coefficient vanishes (i.e., $\rho = 0$), which means that no coupling exists in these two cases. It is also found that ρ is relatively small for materials with positive Poisson's ratio but for auxetic materials with negative Poisson's ratio, it has a relatively large value. This indicates that the coupling effect may be especially significant when the adhesive contact behavior of auxetic materials is considered.

Since the oscillatory stress field is by itself an anomalous result associated with linear elasticity, it is often interesting to consider the solution when the value of ρ is set to zero (Hutchinson and Suo, 1992). Under this circumstance, it can be shown that the corresponding stress field reduces to

$$\begin{aligned} rp_0(r) &= -\left\{\frac{P\Gamma(2+k)}{\pi(2a)^{1+k}[\Gamma(1+k/2)]^2}+\frac{d_{03}a^2}{(3+k)\kappa}\right\}\Omega_1(r)+\frac{d_{03}}{\kappa}\Omega_3(r),\\ q_0(r) &= -(2+k)d_{03}\kappa R\varepsilon r\Omega_1(r), \end{aligned} \tag{22}$$

where

$$d_{03}=\lim_{\rho\to 0}d_3,\quad \Omega_m(r)=\frac{1}{r}\frac{\mathrm{d}}{\mathrm{d}r}\int_r^a\frac{s^m(a^2-s^2)^{\frac{k}{2}}}{\sqrt{s^2-r^2}}\mathrm{d}s\quad (m=1,3). \tag{23}$$

Through some manipulation of analytical integrations, it yields that

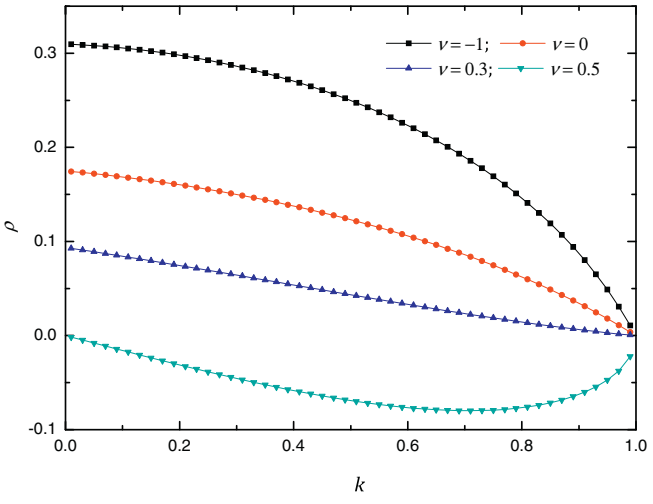

Fig. 2. Variation of the coupling coefficient ρ with respect to the gradient exponent k for different values of Poisson's ratio v.

$$\begin{aligned} \Omega_1(r) &= -\frac{k}{2}\frac{\Gamma(k/2)\sqrt{\pi}}{\Gamma\left(\frac{1+k}{2}\right)}(a^2-r^2)^{\frac{k-1}{2}},\\ \Omega_3(r) &= a^2\Omega_1(r)+\frac{2+k}{2}\frac{\sqrt{\pi}\Gamma(1+k/2)}{\Gamma\left(\frac{3+k}{2}\right)}(a^2-r^2)^{\frac{1+k}{2}}. \end{aligned} \tag{24}$$

Inserting Eq. (24) back into Eq. $(22)_1$, it can be found that

$$p_0(r)=C_1\left[1-\left(\frac{r}{a}\right)^2\right]^{\frac{1+k}{2}}+C_2\left[1-\left(\frac{r}{a}\right)^2\right]^{\frac{k-1}{2}}, \tag{25}$$

where

$$\begin{aligned} C_1 &= \frac{4a^{1+k}E^*\cos(k\pi/2)}{\pi^{\frac{3}{2}}Rc_0^kC_k\beta\sin(\beta\pi/2)}\frac{\Gamma(1+k/2)}{(1+k)\Gamma(1/2+k/2)},\\ C_2 &= \frac{P(1+k)}{2\pi a^2}-\frac{4a^{1+k}E^*\cos(k\pi/2)}{\pi^{\frac{3}{2}}Rc_0^kC_k\beta\sin(\beta\pi/2)}\frac{\Gamma(1+k/2)}{(3+k)\Gamma(1/2+k/2)}. \end{aligned} \tag{26}$$

The normal traction $p_0(r)$ obtained in this way is exactly the same as that in the frictionless case obtained by Chen et al. (2009b) via a superposition of the Hertz solution of a rigid sphere and the solution of a flat-ended cylindrical punch. Note that $p_0(r)$ becomes independent of the mismatch strain ε when $\rho = 0$.

3.2. Indentation depth

Substituting the expression of H_0 in Eq. (15) into Eq. (10) yields the indentation depth as

$$\delta = d_4Pa^{-1-k}+\omega_1\frac{a^2}{R}-\frac{4\kappa\rho a\varepsilon}{2+k}, \tag{27}$$

where

$$d_4=\frac{\kappa\pi\Gamma(2+k)c_0^kC_k\sin(\beta\pi/2)}{2^{2+k}E^*R_t\cosh(\pi\rho)\cos(k\pi/2)},\quad \omega_1=\frac{2+k-4\rho^2}{(3+k)(2+k)}. \tag{28}$$

Taking the limit of $\rho \to 0$, δ reduces to the corresponding solution in the frictionless case,

$$\delta_{\mathrm{frl}}=\lim_{\rho\to 0}\delta=\frac{P\sqrt{\pi}c_0^kC_k\beta\sin(\beta\pi/2)}{4a^{1+k}E^*\cos(k\pi/2)}\frac{\Gamma(1/2+k/2)}{\Gamma(1+k/2)}+\frac{1}{3+k}\frac{a^2}{R}. \tag{29}$$

The interfacial stress distributions and indentation depth for a flat-ended cylindrical punch can also be obtained by following the same procedure mentioned above. Again, in the limit of $\rho \to 0$, the result reduces to the solution to a flat-ended cylindrical rigid punch derived by Giannakopoulos and Suresh (1997b). For the limitation of space, further details are omitted here.

3.3. P–a–ε relation and pull-off force

The elastic strain energy stored in the half-space is

$$U_E = U_{Ep}+U_{Eq}, \tag{30}$$

where

$$\begin{aligned} U_{Ep} &= \frac{1}{2}\int_0^a p(r)\bar{u}_z(r)2\pi r\,\mathrm{d}r=\frac{P}{2}\delta-\frac{\pi}{2R}\int_0^a r^3p(r)\mathrm{d}r,\\ U_{Eq} &= \frac{1}{2}\int_0^a q(r)\bar{u}_r(r)2\pi r\,\mathrm{d}r=\pi\varepsilon\int_0^a q(r)r^2\,\mathrm{d}r. \end{aligned} \tag{31}$$

Meanwhile, it can be shown that

$$\int_0^a r^2\Phi_1'(r)\mathrm{d}r = -\frac{2+k-4\rho^2}{\Gamma(4+k)}2^{1+k}R_t a^{3+k},$$
$$\int_0^a r^2\Phi_3'(r)\mathrm{d}r = -\frac{3(4+k)(2+k)-8\rho^2(10+3k-2\rho^2)}{\Gamma(6+k)}R_t 2^{1+k}a^{5+k},$$
$$\int_0^a r^2\Psi_0'(r)\mathrm{d}r = -\frac{\rho}{\Gamma(3+k)}R_t 2^{2+k}a^{2+k},$$
$$\int_0^a r^2\Psi_2'(r)\mathrm{d}r = -\frac{(8+3k-4\rho^2)\rho}{\Gamma(5+k)}R_t 2^{2+k}a^{4+k}. \tag{32}$$

Combining Eqs. (18), (31) and (32) gives

$$U_{Ep} = \frac{P}{2}\delta - \frac{\omega_1}{2R}Pa^2 + 2^{1+k}\frac{\pi d_3 d_5}{\kappa}\frac{a^{5+k}}{R} + 2^{2+k}\pi d_3 d_6 \varepsilon a^{4+k},$$
$$U_{Eq} = \frac{2\kappa\rho\varepsilon}{2+k}Pa + 2^{2+k}\pi d_3 d_6 \varepsilon a^{4+k} + 2^{1+k}\pi d_3 d_7 \kappa R a^{3+k}\varepsilon^2, \tag{33}$$

where

$$d_5 = \frac{(1+4\rho^2)d_7}{(5+k)(3+k)}, \quad d_6 = \frac{\rho d_7}{4+k}, \quad d_7 = \frac{[(2+k)^2+4\rho^2]R_t}{\Gamma(4+k)} \tag{34}$$

are all dimensionless quantities.

Equilibrium of the adhesive system requires that

$$\left.\frac{\partial U_T}{\partial a}\right|_{\delta,\varepsilon} = \left.\frac{\partial U_{Ep}}{\partial a}\right|_{\delta,\varepsilon} + \left.\frac{\partial U_{Eq}}{\partial a}\right|_{\delta,\varepsilon} - 2\Delta\gamma = 0. \tag{35}$$

Inserting Eq. (33) into Eq. (35), while noting

$$\left.\frac{\partial P}{\partial a}\right|_{\delta,\varepsilon} = (1+k)\frac{P}{a} - \frac{\omega_1}{d_4}\frac{2a^{2+k}}{R} + \frac{4\kappa\rho\varepsilon}{(2+k)d_4}a^{1+k} \tag{36}$$

leads to the following P–a–ε relation in a normalized form

$$\frac{9\omega_0\alpha^k}{2\hat{R}^k}\hat{a}^{3+k} - 6\omega_1\hat{P} + \frac{8\omega_2\hat{R}^k}{\alpha^k}\frac{\hat{P}^2}{\hat{a}^{3+k}} + \frac{9\omega_3}{2}\alpha^k\hat{R}^{1-k}\hat{a}^{2+k}\varepsilon$$
$$+\frac{9\omega_4}{2}\alpha^k\hat{R}^{2-k}\varepsilon^2\hat{a}^{1+k} + 12\omega_5\frac{\hat{R}\hat{P}}{\hat{a}}\varepsilon - 1 = 0, \tag{37}$$

where

$$\omega_0 = \frac{2^{2+k}(1+4\rho^2)}{\beta(3+k)}d_8 d_9, \quad \omega_2 = \frac{\beta\Gamma(2+k)}{2^{4+k}d_8},$$
$$\omega_3 = \frac{2^{4+k}\rho}{1+k}d_8 d_9, \quad \omega_4 = \frac{2^{2+k}(3+k)\kappa}{1+k}d_8 d_9, \quad \omega_5 = \frac{\kappa\rho}{2+k} \tag{38}$$
$$d_8 = \frac{R_t\cosh(\pi\rho)\cos(k\pi/2)}{\pi C_k\sin(\beta\pi/2)}, \quad d_9 = \frac{(2+k)^2+4\rho^2}{(2+k)\Gamma(4+k)}.$$

In Eq. (37),

$$\hat{a} = \frac{a}{a_{\mathrm{JKR}}}, \quad \hat{R} = \frac{R}{a_{\mathrm{JKR}}}, \quad \hat{P} = \frac{3PR}{4E^* a_{\mathrm{JKR}}^3}, \quad \alpha = \frac{R}{c_0} \tag{39}$$

are all dimensionless quantities and $a_{\mathrm{JKR}} = \sqrt[3]{9\pi R^2\Delta\gamma/(2E^*)}$ is the classical JKR contact radius corresponding to $\varepsilon = 0$ and $P = 0$ simultaneously.

The normalized contact radius a/a_{JKR} as a function of the mismatch strain ε for a power-law graded half-space with gradient exponent $k = 0.5$ under different pulling forces is plotted in Fig. 3, where both true and non-oscillatory solutions (obtained by letting $\rho = 0$ artificially) are shown for comparison. It can be seen that the behavior of a/a_{JKR} with respect to ε is qualitatively similar to that in the case of homogeneous materials (Chen and Gao, 2006a,b, 2007b). Fig. 3a and b also shows that the coupling effect tends to reduce the contact area for a given value of the mismatch strain but it becomes more significant for auxetic materials ($\nu = -0.3$) than for regular materials ($\nu = 0.3$).

The P–a–ε relation can also be normalized in another form:

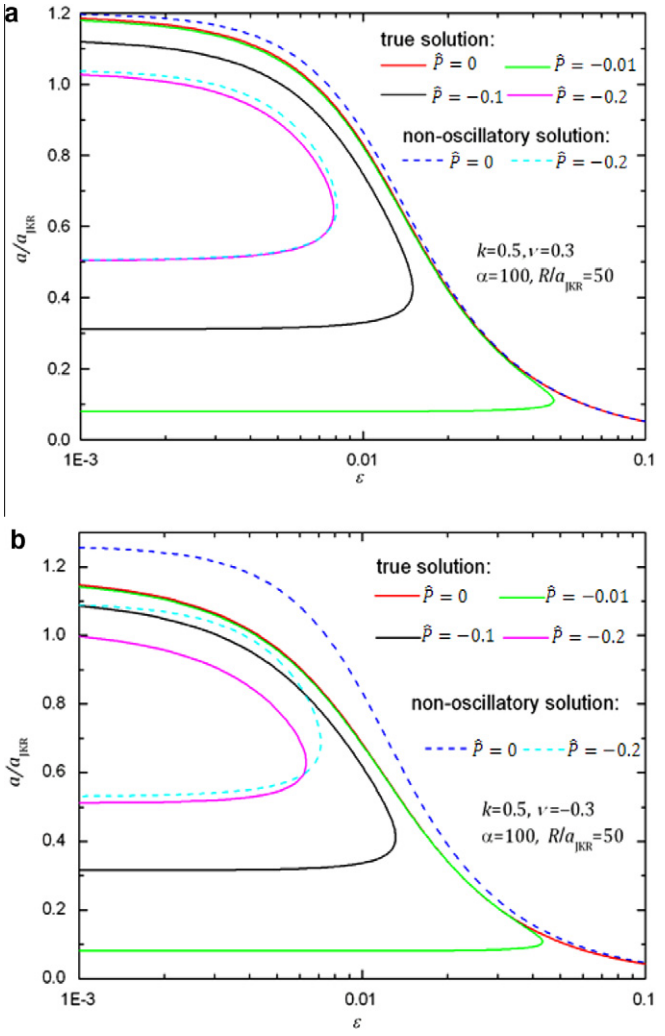

Fig. 3. Variation of the normalized contact radius a/a_{JKR} as a function of the mismatch strain ε for a power-law graded elastic half-space with gradient exponent $k = 0.5$ under different pulling forces.

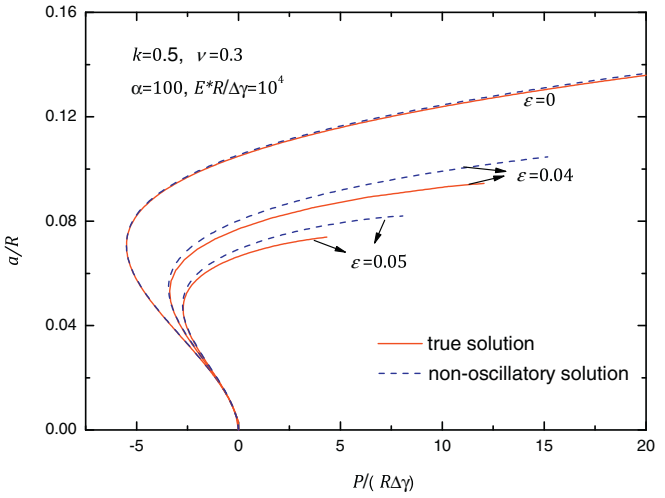

Fig. 4. P–a relation for a power-law graded elastic half-space with gradient exponent $k = 0.5$.

$$\omega_0\tilde{E}\alpha^k\tilde{a}^{3+k} + \left(\frac{2\omega_5\varepsilon}{\tilde{a}} - \omega_1\right)\tilde{P} + \frac{\omega_2}{\tilde{E}\alpha^k\tilde{a}^{3+k}}\tilde{P}^2 + \omega_3\tilde{E}\alpha^k\tilde{a}^{2+k}\varepsilon$$
$$+\omega_4\tilde{E}\alpha^k\tilde{a}^{1+k}\varepsilon^2 - \pi = 0, \tag{40}$$

where

$$\tilde{a}=\frac{a}{R},\quad \widetilde{P}=\frac{P}{R\Delta\gamma},\quad \widetilde{E}=\frac{E^{*}R}{\Delta\gamma}. \tag{41}$$

Fig. 4 shows the normalized contact radius a/R as a function of the normalized load $P/(R\Delta\gamma)$ predicted from Eq. (40) for $k = 0.5$ and $\nu = 0.3$ under different values of the mismatch strain. Both true and non-oscillatory solutions are depicted for comparison. It can be seen that the mismatch strain does have some influence on the contact radius of the adhesion system. The smaller the mismatch strain, the more accurate the non-oscillatory solution.

In the absence of mismatch strain ($\varepsilon = 0$), the P–a relation can be obtained as

$$\widetilde{P}=\left[\omega_1-\sqrt{\omega_1^2-4\omega_0\omega_2+\frac{4\pi\omega_2}{\widetilde{E}\alpha^k\tilde{a}^{3+k}}}\right]\frac{\widetilde{E}\alpha^k}{2\omega_2}\tilde{a}^{3+k}. \tag{42}$$

According to Eq. (42), Fig. 5a and b plots the P–a relations predicted by the current non-slipping contact model and the frictionless contact model by Chen et al. (2009b) for prescribed values of $k, \alpha, \widetilde{E}$ and ν. For materials with $\nu = 0.3$, it can be seen that the two sets of solutions agree well in the tensile regime ($P < 0$) but the non-slipping condition tends to reduce the contact area in the compressive regime ($P > 0$). For auxetic materials with $\nu = -0.3$, the discrepancy between the two models becomes more prominent in the compressive regime ($P > 0$).

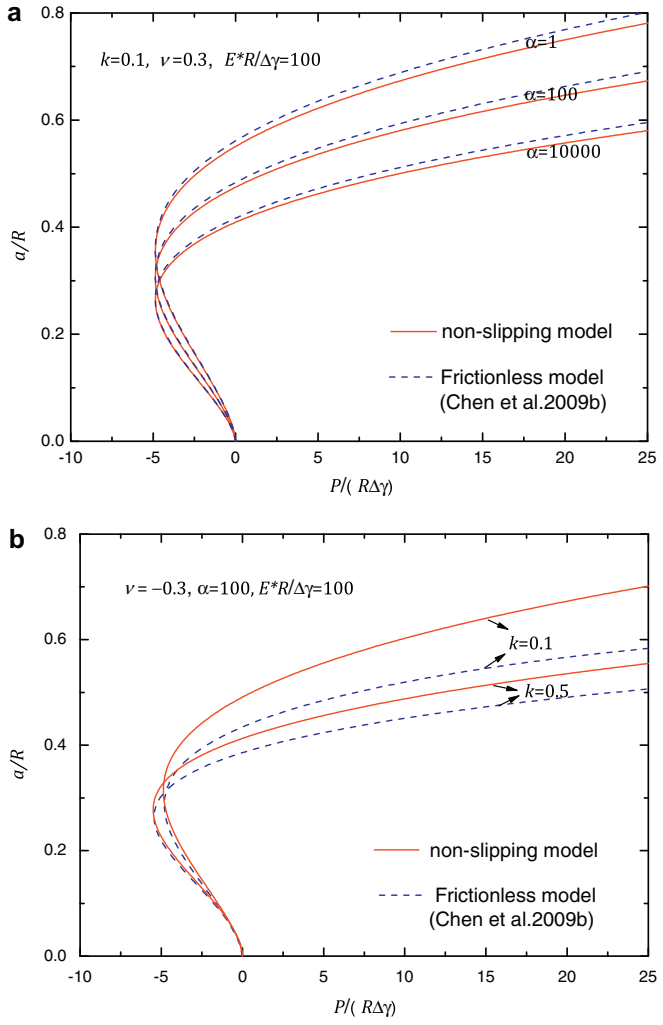

Fig. 5. P–a relation in the absence of mismatch strain predicted by different contact models.

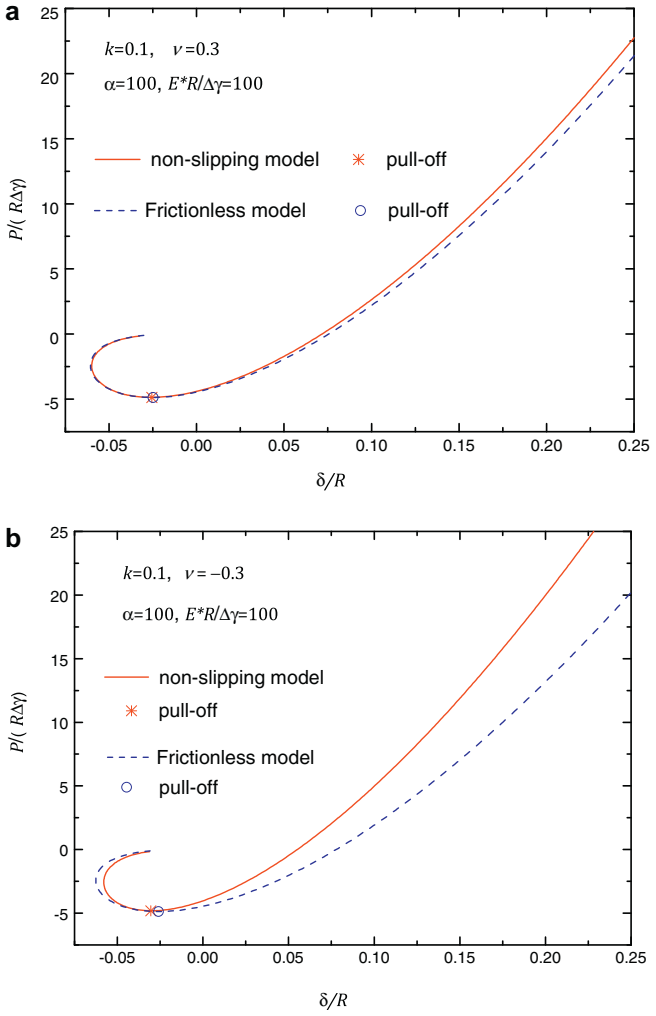

Fig. 6. P–δ relation in the absence of a mismatch strain from non-slipping and frictionless contact models.

It may be also of interest to make a comparison between P–δ relations obtained by non-slipping and frictionless contact models. In the case of $\varepsilon = 0$, Fig. 6a and b shows the normalized load $P/(R\Delta\gamma)$ as a function of the normalized indentation depth δ/R predicted by the two models for $\nu = 0.3$ and $\nu = -0.3$, respectively. One can see that the non-slipping condition tends to reduce the indentation depth until pull-off and the discrepancy between the results obtained by the two models is more obvious for the latter case. This is interesting in view of recent reports that auxetic materials with negative Poisson's ratio, such as polymeric and metallic foams (Chan and Evans, 1998; Lakes and Elms, 1993), carbon fiber composite laminates (Coenen et al., 2001) and microporous polymers (Alderson et al., 2000), exhibit higher resistance to indentation than conventional materials with positive Poisson's ratio. Our analysis thus provides a feasible explanation of this phenomenon.

In the case of $\varepsilon = 0$, the critical force and contact radius at pull-off can be obtained from Eq. (42) as

$$P^{\mathrm{pf}}=-\frac{\pi R\Delta\gamma}{\omega_1+2\sqrt{\omega_0\omega_2}},\quad a^{\mathrm{cr}}=R\left[\frac{\sqrt{\omega_2}\pi\alpha^{-k}}{\sqrt{\omega_0}(\omega_1+2\sqrt{\omega_0\omega_2})}\frac{\Delta\gamma}{E^{*}R}\right]^{\frac{1}{3+k}}. \tag{43}$$

In the frictionless limit of $\rho \to 0$, it can be shown that

$$P^{0pf} = -\frac{3+k}{2}\pi R\Delta\gamma,$$
$$a^{0cr} = R\left[\frac{\pi^{3/2}C_k\beta\sin(\beta\pi/2)}{16\cos(k\pi/2)}\frac{(1+k)(3+k)^2}{\Gamma(1+k/2)}\Gamma\left(\frac{1+k}{2}\right)\frac{\alpha^{-k}\Delta\gamma}{E^*R}\right]^{\frac{1}{3+k}}, \tag{44}$$

which is in perfect agreement with those obtained by Chen et al. (2009b) under the frictionless assumption. Furthermore, the P–a relation in the frictionless case can also be found by letting $\rho \to 0$ in Eq. (42).

In the absence of a mismatch strain, Fig. 7 plots the normalized pull-off force P^{pf}/P^{pf}_{JKR} as a function of the gradient exponent k for different values of ν, along with the corresponding frictionless solution. Here P^{pf}_{JKR} is the pull-off force corresponding to the classical JKR model. It can be observed that for the frictionless case, the pull-off force depends linearly on the gradient exponent k and is independent of the Poisson's ratio of the half-space (Chen et al., 2009b). When the coupling effect is involved, however, the pull-off force exhibits some slight dependence on the Poisson's ratio of the half-space. Even so, the frictionless model can still give a good approximation for the pull-off force. The non-slipping condition causes less than 2.5% reduction in the pull-off force. It is also interesting to note that under the parabolic assumption of the punch shape, the pull-off force is also independent of E_0 even if the non-slipping condition is assumed within the contact region.

4. Generalized JKR solution for homogeneous materials

In this section, we will show that the general solution to non-slipping contact on graded materials can be reduced to the non-slipping JKR solution for homogeneous materials.

4.1. Stress field within the contact zone and the indentation depth

In the homogeneous limit, i.e. $k \to 0$, it can be shown that

$$\beta \to 1, \quad \lambda \to 0, \quad \kappa \to 1, \quad C_k \to 2/\pi, \quad \rho \to \rho_0 = \frac{1}{2\pi}\ln(3-4\nu),$$
$$R_t \to R_t^* = \frac{\pi\rho_0}{\sinh(\pi\rho_0)}, \quad d_3 \to d_3^* = \frac{E^*\cosh(\pi\rho_0)}{\pi R}. \tag{45}$$

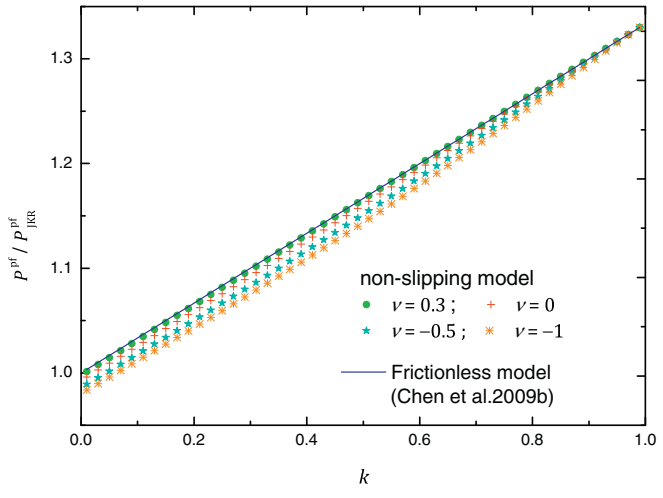

Fig. 7. Normalized pull-off force P^{pf}/P^{pf}_{JKR} as a function of gradient exponent k for various values of Poisson's ratio ν from different contact models without the mismatch strain ($\varepsilon = 0$).

It follows from Eq. (18) that the stress distribution within the contact zone becomes

$$rp_{hom}(r) = -d_1^*\phi_1'(r) + d_3^*\phi_3'(r) + 2d_2^*d_3^*\varphi_2'(r),$$
$$q_{hom}(r) = -d_1^*\varphi_0'(r) + d_3^*\varphi_2'(r) - 2d_2^*d_3^*\phi_1'(r), \tag{46}$$

where

$$d_1^* = \frac{P}{2\pi aR_t^*} + d_3^*\left(\frac{1+4\rho_0^2}{3}a^2 + 2\rho_0\varepsilon Ra\right), \quad d_2^* = \rho_0 a + R\varepsilon \tag{47}$$

and

$$\phi_n'(r) = \frac{d}{dr}\int_r^a \frac{s^n}{\sqrt{s^2-r^2}}\cos\left(\rho_0\ln\frac{a+s}{a-s}\right)ds,$$
$$\varphi_n'(r) = \frac{d}{dr}\int_r^a \frac{s^n}{\sqrt{s^2-r^2}}\sin\left(\rho_0\ln\frac{a+s}{a-s}\right)ds. \tag{48}$$

The depth of indentation can be recovered from Eq. (27) as

$$\delta_{hom} = \frac{P\tanh(\pi\rho_0)}{2\pi\rho_0E^*a} + \frac{(1-2\rho_0^2)a^2}{3R} - 2\rho_0a\varepsilon. \tag{49}$$

For an incompressible half-space ($\nu = 0.5$), we have $\rho_0 = 0$, then

$$p(r) = \frac{E^*}{\pi}\left(\frac{P}{2E^*a^2} - \frac{2a^2}{3R}\right)\frac{1}{\sqrt{a^2-r^2}} + \frac{2E^*}{\pi R}\sqrt{a^2-r^2},$$
$$q(r) = \frac{2E^*\varepsilon}{\pi}\frac{r}{\sqrt{a^2-r^2}}. \tag{50}$$

The stress field given by Eqs. (46) and (50) are consistent with the oscillatory and non-oscillatory solutions for homogeneous materials by Chen and Gao (2006b) when one of the contacting bodies is rigid.

Furthermore, in the absence of a mismatch strain ($\varepsilon = 0$), we have

$$q(r) = 0, \tag{51a}$$
$$p_{JKR}(r) = \frac{E^*}{\pi a}\left(\delta_{JKR} - \frac{a^2}{R}\right)\left[1-\left(\frac{r}{a}\right)^2\right]^{-\frac{1}{2}} + \frac{2E^*a}{\pi R}\left[1-\left(\frac{r}{a}\right)^2\right]^{\frac{1}{2}} \tag{51b}$$

and

$$\delta_{JKR} = \frac{P}{2aE^*} + \frac{a^2}{3R}. \tag{52}$$

These results coincide with the classical JKR solutions (Johnson et al., 1971) for homogeneous materials.

4.2. P–a–ε relation and pull-off force

In the homogeneous limit, $k \to 0$, the corresponding P–a–ε relation from Eq. (37) can be written as

$$\omega_0^*\hat{a}^3 - \frac{4\omega_1^*}{3}\hat{P} + \frac{16\omega_2^*}{9}\hat{P}^2\hat{a}^{-3} + \omega_3^*\alpha^k\hat{R}\varepsilon\hat{a}^2 + \omega_4^*\hat{R}^2\varepsilon^2\hat{a}$$
$$+\frac{8\omega_5^*}{3}\frac{\hat{P}}{\hat{a}}\hat{R}\varepsilon - \frac{2}{9} = 0, \tag{53}$$

where

$$\omega_0^* = \frac{4(1+4\rho_0^2)}{3}d_8^*d_9^*, \quad \omega_1^* = \frac{1-2\rho_0^2}{3}, \quad \omega_2^* = \frac{1}{16d_8^*},$$
$$\omega_3^* = 16\rho_0d_8^*d_9^*,$$
$$\omega_4^* = 12d_8^*d_9^*, \quad \omega_5^* = \frac{\rho_0}{2}, \quad d_8^* = \frac{\pi\rho_0}{2\tanh(\pi\rho_0)}, \quad d_9^* = \frac{1+\rho_0^2}{3}. \tag{54}$$

When $P = 0$ and $\varepsilon = 0$, the equilibrium contact radius a_0 can be obtained as

$$\frac{a_0}{a_{\mathrm{JKR}}}=\left[\frac{\tanh(\pi\rho_0)}{\pi\rho_0(1+\rho_0^2)(1+4\rho_0^2)}\right]^{\frac{1}{3}}, \tag{55}$$

where $a_{\mathrm{JKR}}=\sqrt[3]{9\pi R^2\Delta\gamma/(2E^*)}$ is the self-equilibrium contact radius corresponding to the JKR model and the right hand term in Eq. (55) is a little bit smaller than 1. For incompressible materials ($\rho_0=0$), Eq. (53) is reduced to the following non-oscillatory solution for the P–a–ε relation (Chen and Gao, 2006b)

$$\hat{a}^3+9\widehat{R}^2\varepsilon^2\hat{a}-1+\widehat{P}^2\hat{a}^{-3}-2\widehat{P}=0. \tag{56}$$

Accordingly, in the homogeneous case, Eq. (40) reduces to the following form:

$$\frac{\omega_6\widetilde{P}^2}{8\widetilde{E}\tilde{a}^3}-\frac{1-2\rho_0^2}{3}\widetilde{P}+\frac{2(1+\rho_0^2)(1+4\rho_0^2)}{9\omega_6}\widetilde{E}\hat{a}^3+\frac{\rho_0\widetilde{P}\varepsilon}{\hat{a}}+\frac{8\rho_0(1+\rho_0^2)}{3\omega_6}\widetilde{E}\hat{a}^2\varepsilon+\frac{2(1+\rho_0^2)}{\omega_6}\widetilde{E}\tilde{a}\varepsilon^2-\pi=0, \tag{57}$$

where $\omega_6=\tanh(\pi\rho_0)/(\pi\rho_0)$.

In the absence of ε, the following P–a relation can be obtained as

$$P=\frac{4\pi\rho_0E^*a^3}{R\tanh(\pi\rho_0)}\left[\frac{1-2\rho_0^2}{3}-\sqrt{\frac{\tanh(\pi\rho_0)R^2\Delta\gamma}{2\rho_0E^*a^3}-\rho_0^2}\right]. \tag{58}$$

Consequently, the pull-off force and the corresponding critical contact radius become

$$P_{\mathrm{hom}}^{\mathrm{pf}}=-\frac{3\pi R\Delta\gamma}{1-2\rho_0^2+\sqrt{(1+\rho_0^2)(1+4\rho_0^2)}},$$
$$a_{\mathrm{hom}}^{\mathrm{cr}}=\left\{\frac{\tanh(\pi\rho_0)}{4\rho_0^3}\left[1+\frac{2\rho_0^2-1}{\sqrt{(1+\rho_0^2)(1+4\rho_0^2)}}\right]\frac{R^2\Delta\gamma}{E^*}\right\}^{1/3}. \tag{59}$$

In the frictionless limit ($\rho_0\to 0$), Eq. (57) becomes

$$\widetilde{P}=\frac{4}{3}\widetilde{E}\tilde{a}^3-\sqrt{8\pi\widetilde{E}\tilde{a}^3-16\widetilde{E}^2\varepsilon^2\tilde{a}^4}, \tag{60}$$

which is just the non-oscillatory solution derived by Chen and Gao (2006b). The self-equilibrium contact radius

$$a_{\mathrm{JKR}}=\left(\frac{9\pi R^2\Delta\gamma}{2E^*}\right)^{1/3}, \tag{61}$$

the pull-off force and the critical contact radius

$$P_{\mathrm{JKR}}^{\mathrm{pf}}=-\frac{3\pi}{2}R\Delta\gamma,\quad a_{\mathrm{JKR}}^{\mathrm{cr}}=\left(\frac{9\pi R^2\Delta\gamma}{8E^*}\right)^{1/3} \tag{62}$$

in the classical JKR model can all be recovered by taking ρ_0 in Eqs. (55) and (59).

The above analysis shows that the classical frictionless JKR solution coincides with the non-slipping solution for incompressible materials ($\nu=0.5$). For regular materials with positive Poisson's ratio, as indicated by Chen and Gao (2006b), the JKR solution is very close to the non-slipping solution. For auxetic materials with negative Poisson's ratios, however, there are larger differences between the classical JKR solution and the non-slipping solution.

5. Adhesion mediated deformation sensor

Induced by the changes in environment temperature, the presence of a mismatch strain may cause the adhesion to break up, leading to the concept of adhesion mediated deformation sensor proposed by Chen and Gao (2006b, 2007b). So far this model has only been studied for homogeneous materials, and here we extend it to the power-law graded material. For a fixed mismatch strain with no applied force, the contact radius behaves according to Eq. (37) in which $P=0, a=a_{\mathrm{eq}}$. In this regard, the adhesion energy can be obtained as

$$\Delta U=-U_T\big|_{a=a_{\mathrm{eq}}}^{P=0,\varepsilon\neq 0}=\pi a_{\mathrm{eq}}^2\Delta\gamma-\Delta U_E, \tag{63}$$

where

$$\Delta U_E=2^{1+k}\frac{\pi d_3d_5}{\kappa}\frac{a_{\mathrm{eq}}^{5+k}}{R}+2^{3+k}\pi d_3d_6\varepsilon a_{\mathrm{eq}}^{4+k}+2^{1+k}\pi d_3d_7\kappa R a_{\mathrm{eq}}^{3+k}\varepsilon^2. \tag{64}$$

Fig. 8 plots the normalized adhesion energy $\Delta U/(K_BT)$, where K_B is the Boltzmann constant and $T=300$ K is the room temperature, versus the mismatch strain for various k. At a finite $|\varepsilon|<0.1$, the adhesion energy decreases initially with k until $k=0.5$, then ΔU increases with k monotonically. In addition, ΔU associated with $k>0.5$ is seen to decrease more slowly than that for $k<0.5$. This means that the adhesion system for $k>0.5$ shows more stability than for smaller values of k. Even so, the adhesion energy is reduced to the level of K_BT as $|\varepsilon|\geqslant 0.1$, when adhesion will become sensitive to thermal fluctuations.

6. Effect of mode mixity for graded materials

The above analysis of non-slipping adhesive contact on power-law graded materials is based on the assumption that the work of adhesion $\Delta\gamma$ is a material constant throughout the loading process, as in the case of a perfectly elastic material with reversible adhesion. It is also assumed that $\Delta\gamma$ is independent of the local fracture mode, meaning it does not depend on whether the detachment occurs by tensile or shear failure mode along the interface. However, as demonstrated recently by Waters and Guduru (2010), under combined normal and tangential loading conditions (mixed-mode loading), the work of adhesion increases significantly with increasing degree of mode mixity. This is not difficult to understand if the similarity between fracture mechanics and contact mechanics is recalled (Maugis, 1992; Giannakopoulos et al., 1998) since it is well known in fracture mechanics that mode mixity will increase the interface fracture toughness. Following the ideas from fracture mechanics (Evans et al., 1990; Hutchinson and Suo, 1992), here we investigate the influence of mode mixity on adhesive contact of graded materials. Without loss of generality, we focus attention on plane strain adhesive contact.

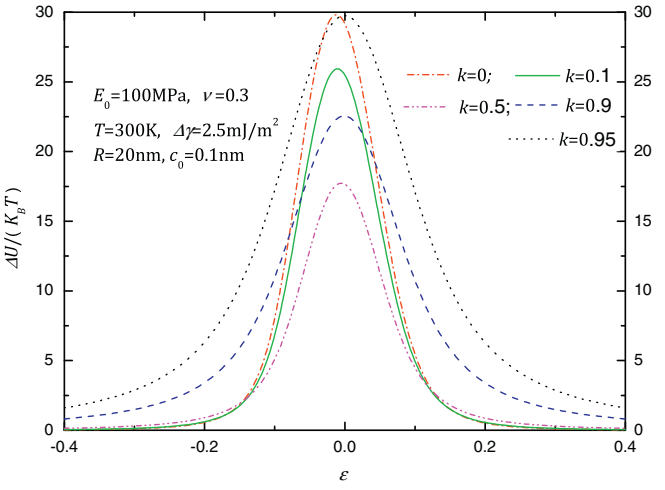

Fig. 8. Variation of the normalized adhesion energy $\Delta U/(K_BT)$ as a function of mismatch strain ε for different values of k.

As shown by Jin and Guo (2010) for a rigid cylinder of radius R in non-slipping adhesive contact with a power-law graded half-space under a normal force P (negative when tensile), the normal (z direction) and tangential (x direction) tractions in the contact region can be expressed as follows (Jin and Guo, 2010)

$$p(x)=\frac{1}{(a^2-x^2)^{\frac{1-k}{2}}}\left\{I_1\cos\left(\rho\ln\frac{a+x}{a-x}\right)-I_2\sin\left(\rho\ln\frac{a+x}{a-x}\right)\right\},$$
$$q(x)=\frac{\kappa}{(a^2-x^2)^{\frac{1-k}{2}}}\left\{I_2\cos\left(\rho\ln\frac{a+x}{a-x}\right)+I_1\sin\left(\rho\ln\frac{a+x}{a-x}\right)\right\}, \tag{65}$$

where

$$I_1=\frac{\Gamma(1+k)}{(2a)^kR_k}P+\frac{1}{\kappa\theta_1R}\frac{a^2(1+4\rho^2)-x^2(2+k)}{(2+k)(1+k)k\sigma_k},$$
$$I_2=\frac{1}{\kappa\theta_1R}\frac{2\rho ax}{(1+k)k\sigma_k} \tag{66}$$

with

$$R_k=\Gamma\left(\frac{1+k}{2}+\mathrm{i}\rho\right)\Gamma\left(\frac{1+k}{2}-\mathrm{i}\rho\right),$$

whilst k, θ_1 and ρ are defined in Eqs. $(6)_2$, $(6)_4$ and $(8)_4$, respectively.

Similar to Erdogan and Wu (1993), we define the complex-valued stress intensity factor for power-law graded materials as follows:

$$K=\sqrt{2\pi}\lim_{x\to a}(a-x)^{\frac{1-k}{2}+\mathrm{i}\rho}\left(p+\frac{\mathrm{i}}{\kappa}q\right)=\sqrt{2\pi}(2a)^{\frac{k-1}{2}+\mathrm{i}\rho}(I_{10}+\mathrm{i}I_{20}), \tag{67}$$

where

$$I_{10}=\frac{\Gamma(1+k)}{(2a)^kR_k}P+\frac{a^2}{\kappa\theta_1R}\frac{4\rho^2-1-k}{(2+k)(1+k)k\sigma_k},$$
$$I_{20}=\frac{a^2}{\kappa\theta_1R}\frac{2\rho}{(1+k)k\sigma_k}. \tag{68}$$

From Eq. (65), the combined interfacial traction at $x=a-\eta$ inside the contact region is

$$\left(p+\frac{\mathrm{i}}{\kappa}q\right)\Big|_{x=a-\eta}=\frac{K}{\sqrt{2\pi}}\eta^{\frac{k-1}{2}-\mathrm{i}\rho}. \tag{69}$$

Moreover, the complex form of the displacement discontinuity ahead of the contact region can be calculated as

$$[u_z]+\mathrm{i}\kappa[u_x]=(u_z+\mathrm{i}\kappa u_x)+\frac{x^2}{2R}-h, \tag{70}$$

where the depth of penetration h is given by

$$h=\frac{\theta_1\sigma_k\kappa\Gamma(1+k)}{(2a)^kR_k}P-\frac{1+k-4\rho^2}{2(1+k)(2+k)}\frac{a^2}{R} \tag{71}$$

with

$$\sigma_k=-\pi[\tan(\beta\pi/2)+\mathrm{i}]/\cos[\pi(k/2+\mathrm{i}\rho)] \tag{72}$$

and β is defined in Eq. $(6)_3$.

From the surface Green's function of power-law graded half-space, the complex surface displacement at $x=a+\eta$ outside the contact region can be obtained as

$$u_z+\mathrm{i}\kappa u_x=-\kappa\theta_1\left(\tan\frac{\beta\pi}{2}+\mathrm{i}\right)\int_{-a}^{a}\frac{p(s)+\frac{\mathrm{i}}{\kappa}q(s)}{(a+\eta-s)^k}\mathrm{d}s. \tag{73}$$

An asymptotic analysis will show that, as $\eta\to0^+$,

$$\int_{-a}^{a}\frac{(a+s)^{\frac{k-1}{2}+\mathrm{i}\rho}(a-s)^{\frac{k-1}{2}-\mathrm{i}\rho}}{(a+\eta-s)^k}\mathrm{d}s$$
$$\to\frac{\pi}{\cos[\pi(k/2+\mathrm{i}\rho)]}-\frac{2kR_k}{(1-k-2\mathrm{i}\rho)\Gamma(1+k)}\left(\frac{\eta}{2a}\right)^{\frac{1-k}{2}-\mathrm{i}\rho},$$
$$\int_{-a}^{a}\frac{s(a+s)^{\frac{k-1}{2}+\mathrm{i}\rho}(a-s)^{\frac{k-1}{2}-\mathrm{i}\rho}}{(a+\eta-s)^k}\mathrm{d}s$$
$$\to\frac{a\pi(k+2\mathrm{i}\rho)}{\cos[\pi(k/2+\mathrm{i}\rho)]}-\frac{2akR_k}{(1-k-2\mathrm{i}\rho)\Gamma(1+k)}\left(\frac{\eta}{2a}\right)^{\frac{1-k}{2}-\mathrm{i}\rho},$$
$$\int_{-a}^{a}\frac{s^2(a+s)^{\frac{k-1}{2}+\mathrm{i}\rho}(a-s)^{\frac{k-1}{2}-\mathrm{i}\rho}}{(a+\eta-s)^k}\mathrm{d}s$$
$$\to\frac{a^2\pi(1+k^2-4\rho^2+4\mathrm{i}k\rho)}{2\cos[\pi(k/2+\mathrm{i}\rho)]}-\frac{2a^2kR_k}{(1-k-2\,\mathrm{i}\rho)\Gamma(1+k)}\left(\frac{\eta}{2a}\right)^{\frac{1-k}{2}-\mathrm{i}\rho}. \tag{74}$$

Combining Eqs. (65)–(74), the asymptotic displacement discontinuity outside of the contact edge is obtained as

$$([u_z]+\mathrm{i}\kappa[u_x])|_{x=a+\eta}=\frac{2\kappa\theta_1[\tan(\beta\pi/2)+\mathrm{i}]kR_k}{(1-k-2\,\mathrm{i}\rho)\Gamma(1+k)}\frac{K}{\sqrt{2\pi}}\eta^{\frac{1-k}{2}-\mathrm{i}\rho}. \tag{75}$$

Based on the above results, the strain energy $\mathrm{d}U_E$ released for a perturbation $\mathrm{d}a$ can be calculated as

$$\mathrm{d}U_E=\frac{1}{2}\int_0^{\mathrm{d}a}\overline{[p+\ \mathrm{i}q/\kappa]}\{[u_z]+\mathrm{i}\kappa[u_x]\}\mathrm{d}\eta$$
$$=\frac{\kappa\theta_1[\tan(\beta\pi/2)+\mathrm{i}]kR_k}{(1-k-2\,\mathrm{i}\rho)\Gamma(1+k)}\frac{|K|^2}{2\pi}\int_0^{\mathrm{d}a}\left(\frac{\eta}{\mathrm{d}a-\eta}\right)^{\frac{k-1}{2}+\mathrm{i}\rho}\mathrm{d}\eta$$
$$=-\frac{\kappa\theta_1k\sigma_kR_k}{4\pi\Gamma(1+k)}|K|^2\mathrm{d}a, \tag{76}$$

Consequently, the energy release rate is

$$G=-\frac{\mathrm{d}U_E}{\mathrm{d}a}=\frac{1}{2}\frac{\kappa\theta_1k\sigma_kR_k}{2\pi\Gamma(1+k)}|K|^2, \tag{77}$$

which is exactly the same as the result given by Jin and Guo (2010) obtained through global energy analysis. In the homogeneous limit, i.e. $k\to0$, we have

$$\kappa\to1,\quad\theta_1\to\frac{1-2\nu}{2(1-\nu)E^*},\quad k\sigma_k\to\frac{2\sqrt{3-4\nu}}{1-2\nu},$$
$$R_k\to\frac{\pi\sqrt{3-4\nu}}{2(1-\nu)},$$

which means that the corresponding energy release rate reduces to the classical result for homogeneous materials (Rice, 1988)

$$G=\frac{1}{2}\frac{1}{\cosh^2(\pi\rho_0)}\frac{|K_0|^2}{E^*}, \tag{79}$$

where ρ_0 is defined in Eq. $(45)_5$ and $K_0=\lim_{k\to0}K$ is the complex stress intensity factor for homogeneous materials. Note that the factor 1/2 appearing in Eqs. (77) and (79) is due to the presence of the rigid punch (Maugis, 1992). The above analysis demonstrates the rationality of the proposed definition of complex-valued stress intensity factor for power-law graded materials.

Following Hutchinson and Suo (1992), we choose the following expression to describe the effect of mode mixity on the work of adhesion

$$\omega_{\mathrm{ad}}(\psi)=\Delta\gamma\xi(\psi)=\frac{\Delta\gamma}{1-(1-\lambda_0)\sin^2\psi}, \tag{80}$$

where $\Delta\gamma$ is the work of adhesion for pure mode I loading; the phenomenological parameter $\lambda_0(0\leqslant\lambda_0\leqslant1)$ adjusts the influence of mode mixity, whose value can be determined from experiments

as discussed in Waters and Guduru (2010). The smaller the value of λ_0, the stronger the effect of mode mixity. When $\lambda_0 = 1$, ω_{ad} reduces to $\Delta\gamma$. In Eq. (80), the mode-mixity angle is defined as

$$\psi = \tan^{-1}\frac{\mathrm{Im}[Kl^{-i\rho}]}{\mathrm{Re}[Kl^{-i\rho}]}, \tag{81}$$

where l is a reference length, the choice of which was discussed by Hutchinson and Suo (1992). As a consequence, the energy balance equation in the adhesive contact analysis can be stated as

$$G = -\frac{dU_E}{da} = \omega_{ad}(\psi). \tag{82}$$

From Eq. (82), the relation between the normalized normal load $P/\Delta\gamma$ and the normalized contact half-width a/R can be written as

$$\frac{k\omega_7\sigma_k\Gamma(1+k)\kappa}{2^{1+k}R_k\alpha^k}\frac{\Delta\gamma}{E^*R}\left(\frac{P}{\Delta\gamma}\right)^2\left(\frac{a}{R}\right)^{-(1+k)} - \omega_8\frac{a}{R}\frac{P}{\Delta\gamma} + \frac{2^{k-1}\omega_9R_k\alpha^k}{\omega_3k\sigma_k\kappa}\frac{E^*R}{\Delta\gamma}\left(\frac{a}{R}\right)^{3+k} - 2\xi(\psi) = 0, \tag{83}$$

where three dimensionless parameters ω_7, ω_8 and ω_9 are defined as

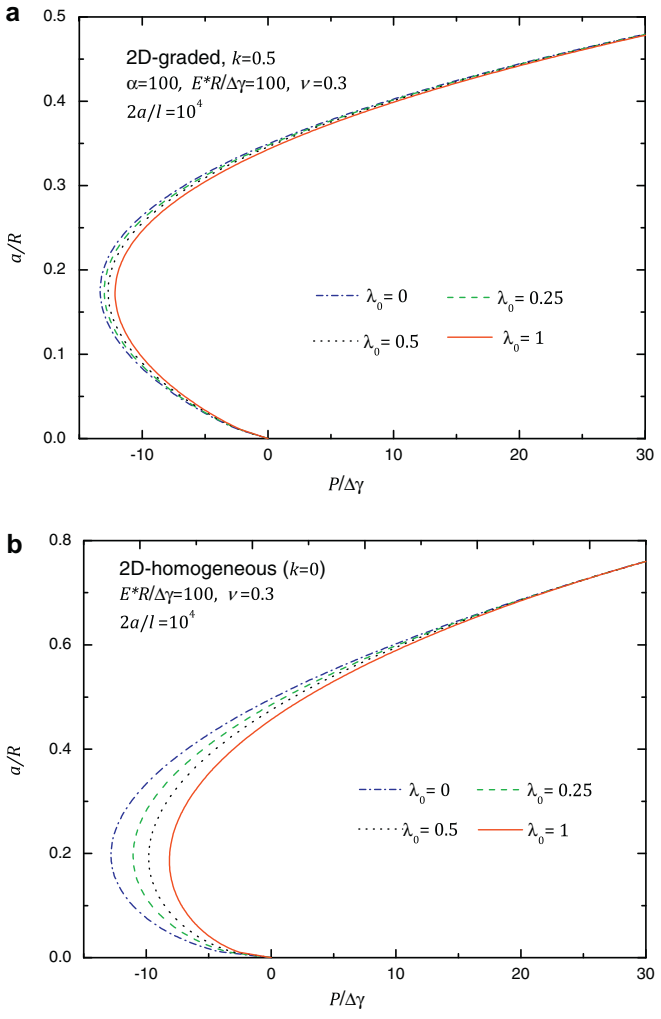

Fig. 9. Normalized contact half-width a/R as a function of the normalized normal load $P/\Delta\gamma$ under different values of the mode-mixity parameter λ_0 for (a) power-law graded half-space ($k = 0.5$) and (b) homogeneous half-space.

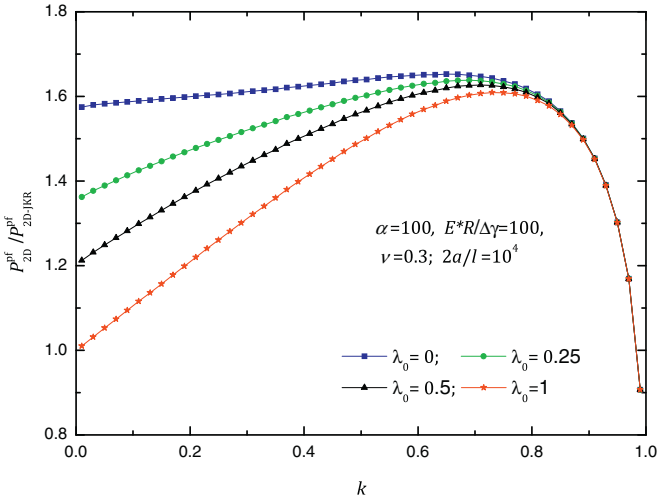

Fig. 10. Normalized pull-off force as a function of the gradient exponent k for different values of λ. $P^{pf}_{2D\text{-}JKR}$ is the pull-off force of the two-dimensional JKR model.

$$\omega_7 = -\frac{C_k}{k}\cos\frac{\beta\pi}{2}, \quad \omega_8 = \frac{1+k-4\rho^2}{(1+k)(2+k)},$$
$$\omega_9 = \frac{(1+4\rho^2)[(1+k)^2+4\rho^2]}{(1+k)(2+k)\Gamma(3+k)}. \tag{84}$$

In the homogeneous limit, i.e. $k \to 0$, Eq. (83) reduces to

$$\frac{1}{\pi}\frac{\Delta\gamma}{E^*R}\left(\frac{P}{\Delta\gamma}\right)^2\left(\frac{a}{R}\right)^{-1} - \frac{1-4\rho_0^2}{2}\frac{a}{R}\frac{P}{\Delta\gamma} + \frac{\pi(1+4\rho_0^2)^2}{16}\frac{E^*R}{\Delta\gamma}\left(\frac{a}{R}\right)^3 - 2\xi(\psi) = 0. \tag{85}$$

According to Eq. (83), Fig. 9a and b plots the variation of a/R as a function of $P/\Delta\gamma$ for graded and homogeneous materials under different values of λ_0, showing qualitatively similar results for various λ_0. This is consistent with the conclusion given by Chen et al. (2009) for peeling of a spatula pad on a homogeneous substrate. For a given value of P, the larger the value of λ_0, the smaller the contact radius. Moreover, for the materials examined ($\nu = 0.3$), the pull-off force increases with decreasing λ_0, which can be observed more clearly from Fig. 10. This indicates that the mode mixity has a more significant effect for homogenous materials than for graded materials. Our analytical model shows that the effect of model mixity can be neglected when the gradient exponent k is greater than 0.8.

7. Conclusions

In the present paper, we have studied non-slipping adhesive contact between a rigid punch with a parabolic shape and a power-law graded elastic half-space based on the Jacobi polynomial method. A series of closed-form analytical solutions are obtained by solving a set of coupled singular integral equations. Our analysis identifies a dimensionless parameter ρ which governs the non-slipping effect, which vanishes in the case of linearly graded materials as well as homogeneous incompressible materials. Our analysis indicates that the frictionless solutions work well for materials with positive Poisson's ratio. However, for materials with negative Poisson's ratio (auxetic materials), the solutions derived under non-slipping condition deviate significantly from the frictionless solutions. Furthermore, the role of mode mixity in plane strain adhesive contact of power-law graded materials has been discussed in some detail, with results showing that the mode

mixity plays a more prominent role for homogenous materials than for graded materials.

In the present analysis, we have considered non-slipping adhesive contact on a power-law graded elastic half-space. This may not be too restrictive since the power-law solutions for $E = E_0(z/c_0)^k$ can sometimes be superposed on the homogeneous solutions to obtain first order solutions for more general cases (Giannakopoulos and Pallot, 2000). It may also be possible to follow a moduli-perturbation approach described in Gao (1991) to obtain some more general approximate solutions based on the present solutions.

Acknowledgements

Financial supports from the National Natural Science Foundation of China (10925209, 10772037), Fundamental Research Funds for the Central Universities (DUT11ZD104) and the National Key Basic Research Special Foundation of China (2006CB601205) are gratefully acknowledged.

References

Alderson, K.L., Fitzgerald, A.F., Evans, K.E., 2000. The strain dependent indentation resilience of auxetic microporous polyethylene. J. Mater. Sci. 35, 4039–4047.
Baney, J.M., Hui, C.Y., 1997. A cohesive zone model for the adhesion of cylinders. J. Adhesion Sci. Technol. 11, 393–406.
Barquins, M., 1988. Adherence and rolling kinetics of a rigid cylinder in contact with a natural rubber surface. J. Adhesion 26, 1–12.
Barthel, E., 1998. On the description of the adhesive contact of spheres with arbitrary interaction potentials. J. Colloid Interface Sci. 200, 7–18.
Booker, J.R., Balaam, N.P., Davis, E.H., 1985a. The behavior of an elastic non-homogeneous half-space. Part I: Line and point loads. Int. J. Numer. Anal. Methods Geomech. 9, 353–367.
Booker, J.R., Balaam, N.P., Davis, E.H., 1985b. The behavior of an elastic non-homogeneous half-space. Part II: Circular and strip footings. Int. J. Numer. Anal. Methods Geomech. 9, 369–381.
Calladine, C.R., Greenwood, J.A., 1978. Line and point loads on a non-homogeneous incompressible elastic half-space. Q. J. Appl. Math. 28, 507–529.
Chan, N., Evans, K.E., 1998. Indentation resilience of conventional and auxetic foams. J. Cell. Plast. 34, 231–262.
Chaudhury, M.K., Weaver, T., Hui, C.Y., Kramer, E.J., 1996. Adhesion contact of cylindrical lens and a flat sheet. J. Appl. Phys. 80, 30–37.
Chen, B., Wu, P., Gao, H., 2009. Pre-tension generates strongly reversible adhesion of a spatula pad on substrate. J. R. Soc. Interface 6, 529–537.
Chen, S., Gao, H., 2006a. Non-slipping adhesive contact of an elastic cylinder on stretched substrates. Proc. R. Soc. Lond. A 462, 211–228.
Chen, S., Gao, H., 2006b. Non-slipping adhesive contact between mismatched elastic spheres: a model of adhesion mediated deformation sensor. J. Mech. Phys. Solids 54, 1548–1567.
Chen, S., Gao, H., 2007a. Bio-inspired mechanics of reversible adhesion: Orientation-dependent adhesion for non-slipping adhesive contact with transversely isotropic elastic materials. J. Mech. Phys. Solids 55, 1001–1015.
Chen, S., Gao, H., 2007b. Non-slipping adhesive contact between mismatched elastic cylinders. Int. J. Solids Struct. 44, 1939–1948.
Chen, S., Yan, C., Soh, A., 2009a. Adhesive behavior of two-dimensional power-law graded materials. Int. J. Solids Struct. 46, 3398–3404.
Chen, S., Yan, C., Zhang, P., Gao, H., 2009b. Mechanics of adhesive contact on a power-law graded elastic half-space. J. Mech. Phys. Solids 57, 1437–1448.
Choi, I.S., Dao, M., Suresh, S., 2008. Mechanics of indentation of plastically graded materials. I: Analysis. J. Mech. Phys. Solids 56, 157–171.
Coenen, V., Alderson, K., Myler, P., Holmes, K., 2001. The indentation response of auxetic composite laminates. In: 6th International Conference on Deformation and Fracture of Composites, Manchester.
Derjaguin, B.V., Muller, V.M., Toporov, Y.P., 1975. Effect of contact deformations on the adhesion of particles. J. Colloid Interface Sci. 53, 314–326.
Donnet, C., Erdemi, A., 2004. Historical developments and new trends in tribological and solid lubricant coatings. Surf. Coat. Technol., 76–84.
Enomoto, Y., Yamamoto, T., 1998. New materials in automotive tribology. Tribol. Lett. 5, 13–24.
Erdogan, F., Wu, B., 1993. Interface crack problems in layered orthotropic materials. J. Mech. Phys. Solids 41, 889–917.
Evans, A.G., Ruhle, M., Dalgleish, B.J., Charalambides, P.G., 1990. The fracture energy of bimaterial interfaces. Mater. Sci. Eng. A 126, 53–64.
Gao, H.J., 1991. Fracture analysis of nonhomogeneous materials via a moduli-perturbation approach. Int. J. Solids Struct. 27, 1663–1682.
Giannakopoulos, A.E., Pallot, P., 2000. Two-dimensional contact analysis of elastic graded materials. J. Mech. Phys. Solids 48, 1597–1631.
Giannakopoulos, A.E., Lindley, T.C., Suresh, S., 1998. Aspects of equivalence between contact mechanics and fracture mechanics: theoretical connections and a life-prediction methodology for fretting-fatigue. Acta Mater. 46, 2955–2968.
Giannakopoulos, A.E., Suresh, S., 1997a. Indentation of solids with gradients in elastic properties. Part I: Point force. Int. J. Solids Struct. 34, 2357–2392.
Giannakopoulos, A.E., Suresh, S., 1997b. Indentation of solids with gradients in elastic properties. Part II: Axisymmetric indentors. Int. J. Solids Struct. 34, 2393–2428.
Gibson, R.E., 1967. Some results concerning displacements and stresses in a non-homogeneous elastic half-space. Geotechnique 17, 58–67.
Gibson, R.E., Sills, G.C., 1975. Settlement of a trip load on a non-homogeneous orthotropic incompressible elastic half-space. Q. J. Appl. Math. 28, 233–243.
Greenwood, J.A., 1997. Adhesion of elastic spheres. Proc. R. Soc. Lond. A 453, 1277–1297.
Hedia, H.S., Nemat-Alla, M., 2004. Design optimization of functionally graded dental implant. Bio-Med. Mater. Eng. 14, 133–143.
Holl, D.L., 1940. Stress transmission in earths. Proc. High Res. Board 20, 709–721.
Hui, C.Y., Lin, Y.Y., Baney, J.M., Kramer, E.J., 2001. The mechanics of contact and adhesion of periodically rough surfaces. J. Polym. Sci., Part B: Polym. Phys. 39, 1195–1214.
Hutchinson, J.W., Suo, Z., 1992. Mixed mode cracking in layered materials. Adv. Appl. Mech. 29, 63–191.
Jin, F., Guo, X., 2010. Non-slipping adhesive contact of a rigid cylinder on an elastic power-law graded half-space. Int. J. Solids Struct. 47, 1508–1521.
Johnson, K.L., 1985. Contact Mechanics. Cambridge University Press, Cambridge.
Johnson, K.L., Kendall, K., Roberts, A.D., 1971. Surface energy and the contact of elastic solids. Proc. R. Soc. Lond. A 324, 301–313.
Kambe, M., Shikata, H., 2003. Intensive energy density thermoelectric energy conversion system by using FGM compliant pads. Acta Astron. 51, 161–171.
Kato, K., Kurimoto, M., Shumiya, H., Adachi, H., Sakuma, S., Okubo, H., 2006. Application of functionally graded material for solid insulator in gaseous insulation system. IEEE Trans. Dielect. Electr. Insul. 13, 363–372.
Lakes, R.S., Elms, K.J., 1993. Indentability of conventional and negative Poisson's ratio foams. J. Comput. Mater. 27, 1193–1202.
Lekhnitskii, S.G., 1962. Radial distribution of stresses in a wedge and in a half-plane with variable modulus of elasticity. PMM 26, 146–151.
Li, X.R., Xie, J.W., Lipner, J., Yuan, X.Y., Thomopoulos, S., Xia, Y.N., 2009. Nanofiber scaffolds with gradations in mineral content for mimicking the tendon-to-bone insertion site. Nano Lett. 9, 2763–2768.
Maugis, D., 1992. Adhesion of spheres: the JKR-DMT transition using a Dugdale model. J. Colloid Interface Sci. 150, 243–269.
Nemat-Alla, M., 2003. Reduction of thermal stresses by developing two-dimensional functionally graded materials. Int. J. Solids Struct. 40, 7339–7356.
Pindera, M., Aboudi, J., Arnold, S.M., 1998. Thermomechanical analysis of functionally graded thermal barrier coatings with different microstructural scales. J. Am. Ceram. Soc. 81, 1525–1536.
Pompe, W., Worch, H., Epple, M., Friess, W., Gelinsky, M., Greil, P., Hempel, U., Scharnweber, D., Schulte, K., 2003. Functionally graded materials for biomedical applications. Mater. Sci. Eng. A 362, 40–60.
Popov, G.Ia., 1973. Axisymmetric contact problem for an elastic inhomogeneous half-space in the presence of cohesion. PMM 37, 1109–1116.
Prasad, A., Dao, M., Suresh, S., 2009. Steady-state frictional sliding contact on surfaces of plastically graded material. Acta Mater. 57, 511–524.
Rice, J.R., 1988. Elastic fracture mechanics concepts for interfacial cracks. J. Appl. Mech. 55, 98–103.
Sioh, E.L., 2010. Functional graded material with nano-structured coating for protection. Int. J. Mater. Prod. Technol. 39, 136–147.
Suresh, S., 2001. Graded materials for resistance to contact deformation and damage. Science 292, 2447–2451.
Suresh, S., Mortensen, A., 1998. Fundamentals of Functionally Graded Materials. Institute of Materials, London.
Waters, J.F., Guduru, P.R., 2010. Mode-mixity-dependent adhesive contact of a sphere on a plane surface. Proc. R. Soc. Lond. A 466, 1303–1325.
Williams, M.L., 1959. The stresses around a fault or crack in dissimilar media. Bull. Seismol. Soc. Am. 49, 199–204.